

Tailoring magnetic and hyperthermia properties of biphase iron oxide nanocubes through post-annealing

Supun B. Attanayake¹, Amit Chanda¹, Raja Das², Manh-Huong Phan¹,
and Hariharan Srikanth^{1,*}

¹Department of Physics, University of South Florida, Tampa, FL 33620, USA

²SEAM Research Centre, South East Technological University, Waterford, Ireland

Tailoring the magnetic properties of iron oxide nanosystems is essential to expand their biomedical applications. In this study, the 34 nm iron oxide nanocubes with two phases consisting of Fe₃O₄ and α -Fe₂O₃ were annealed for 2 hours in the presence of O₂, N₂, He, and Ar to tune the respective phase volume fractions and control the magnetic properties. X-ray diffraction and magnetic measurements were carried out post-treatment to evaluate the changes of the treated samples compared to the as-prepared, which showed an enhancement of the α -Fe₂O₃ phase in the samples annealed with O₂, while the others indicated Fe₃O₄ enhancement. Furthermore, the latter samples indicated enhancements in the crystallinity and saturation magnetization while coercivity enhancement was most significant in the samples annealed with O₂, resulting in the highest specific absorption rates (up to 1000 W/g) in all the applied fields of 800, 600, and 400 Oe in agar during magnetic hyperthermia measurements. The general enhancement in the specific absorption rate post-annealing underscores the importance of the annealing atmosphere in the enhancement of the magnetic and structural properties of nanostructures.

Keywords: Iron oxide nanocubes; Phase tunability; Magnetic hyperthermia; Biomedicine

*Corresponding author: sharihar@usf.edu

1. Introduction

The recent ability to fabricate magnetic structures of nanometer size, known as nanomagnetism, has allowed for the study of unique magnetic phenomena that are unobservable at larger length scales.¹⁻⁴ It has been shown that by utilizing nanostructures with varying sizes and shapes, their applicability in fields ranging from biomedicine to memory devices can be improved.⁵⁻¹¹ Iron oxide, one of the most historically studied magnetic systems has been found to be a unique platform to observe the interplay between different thermodynamically stable phases and their respective magnetic order, which has allowed for broad applications.^{3,12-16} The already Food and Drug Administration (FDA)-approved composition is observed in many of the devices and has shown the potential to be tuned within its iron oxide composition to multiple magnetic phases with distinct features, thus the phase-tunability of iron oxide phases such as magnetite (Fe_3O_4), hematite ($\alpha\text{-Fe}_2\text{O}_3$), maghemite ($\gamma\text{-Fe}_2\text{O}_3$), Wüstite (FeO), etc. are currently being examined.^{17,18} The phase-tunability of iron oxide nanostructures with size has shed light on the stability of certain phases in a variety of conditions, such as the FeO phase which possesses a higher stability in smaller structures of ~ 30 nm.¹⁹ As an extension of an initial study of how the stability of iron oxide phases changes with size, different types of phase tunability in iron oxide nanostructures need to be explored. Prior research has shown that functionalizing iron oxide nanostructures for hyperthermia applications requires the tuning of their shape and size.^{8,20} Of the various shapes that have been previously studied, nanocube structures of size ~ 30 nm have been shown to possess an elevated potential as compared to other structures such as spheres.⁸ This is due to their enhanced anisotropy which results in higher specific absorption rates (SAR) and higher contrasts in magnetic resonance imaging (MRI) in comparison to its spherical counterparts.^{7,8,20,21} Nature itself has shown the importance of contemplating iron oxide nanocubes with structures such as magnetosomes, found within magnetotactic bacteria which possess the capability to act as a

compass utilizing the earth's magnetic field to navigate, opening up its use for further applications spanning from drug delivery to nanoelectronics.²²⁻²⁴

In this study, we explored the effects of annealing atmosphere to manipulate phase volume and hence magnetic properties of biphasic iron oxide nanocubes for biomedical applications. Nanocubes consisting of Fe_3O_4 and $\alpha\text{-Fe}_2\text{O}_3$ with no observable exchange bias or superparamagnetic behavior were annealed in the presence of O_2 , N_2 , He, and Ar to observe compositional and magnetic changes. Herein, O_2 is a reactive gas that can directly interact with iron oxide structures while N_2 is a comparatively less reactive gas that can facilitate reaction-stimulating environments. The latter two gases are well-known inert gases with He being the lightest. Furthermore, the as-prepared and treated nanocubes were evaluated for their effectiveness in magnetic hyperthermia therapy, which showed that the coercivity enhancement plays a major role in tuning hyperthermia efficiency in comparison to the saturation magnetization enhancement.

2. Experiment

Synthesis of iron oxide nanocubes (NCs) was carried out following the procedures put forward by Nemati *et al.*⁸ The chemicals Fe(III)-acetylacetonate ($\text{Fe}(\text{acac})_3$, $\geq 99.9\%$), oleylamine (OA, 70%), oleic acid (OY, 90%), benzyl ether (BE, 98%), and 1,2-hexadecanediol (HDD, 90%) (Sigma-Aldrich, St. Louis, MO, USA) were uniformly mixed using a magnetic stirrer, in a three-necked round-bottomed flask with a jacketed heating mantle. The side openings were dedicated to a thermometer and continuous N_2 flow which was initially carried out with the condenser detached at the first stage, to facilitate degassing for 30 minutes at 110°C to ensure moisture and air are removed out of the flask. The condenser was then fitted with cold water circulation to ensure maximum retainment of the reactants throughout the process. Then the nucleation stage was initiated at 200°C , for 120 minutes with the final reflux stage

carried out for 45 minutes, after which the solution is let to reach room temperature in the absence of a heat source. The obtained turbid reddish solution was then cleaned a minimum of two times with ethanol and a slight amount of hexane. The cleaning is carried out by back-to-back sonication and centrifuging of the solution, each time after the supernatant is disposed of. The obtained product was then let to dry to a fine powder which was evaluated for its structural and morphological characterization using a FEI Morgagni 268 transmission electron microscope (TEM) (FEI, Hillsboro, OR, USA) operating at 60 kV and was followed by compositional evaluation via diffractometry using a Bruker AXS D8 x-ray diffractometer (XRD) (Bruker, Madison, WI, USA) functional in Bragg-Brentano geometry at Cu K α wavelength. The obtained samples which conform to the initial structural and compositional evaluation were then separated, with some kept as controlled while the others were heated in the presence of multiple gases at 300 °C for 2 hours in a ceramic combustion boat placed inside a tube furnace. The gases Oxygen (O₂), Nitrogen (N₂), Helium (He), and Argon (Ar) of ultra-high purity grade were obtained from nexAir. The treated samples were then again evaluated for their structural and morphological characterization using the TEM and XRD. All the magnetic measurements were performed in a DynaCool Physical Property Measurement System (PPMS) (Quantum Design, San Diego, CA, USA), utilizing the vibrating sample magnetometer (VSM) option. Magnetic hyperthermia measurements were performed by using a 4.2 kW Ambrell EasyHeat Li3542 system with varying magnetic fields (0-800 Oe) at a constant 310 kHz frequency. Samples were measured at 20 °C as the starting temperature for a period of 300 seconds at 1 mg/mL nanoparticles in a 2% by-weight agar solution prepared using deionized water.

3. Results and Discussion

3.1. Structural Characterization

The structural and morphological properties of the iron oxide nanocubes (NCs) were evaluated using a transmission electron microscope (TEM), which yielded a size distribution of nanocubes at 34 ± 4 nm. The as-prepared sample (AP) in the inset of Fig. 1(a) displays the uniform distribution of nanocubes which showed the presence of both ferrimagnetic (FiM) magnetite (Fe_3O_4) and antiferromagnetic (AFM) hematite ($\alpha\text{-Fe}_2\text{O}_3$) as seen in the X-ray diffractometry (XRD). When the AP samples were exposed to O_2 , peaks related to $\alpha\text{-Fe}_2\text{O}_3$ further increased, indicating the $\alpha\text{-Fe}_2\text{O}_3$ volume fraction increment. The exposure to N_2 has removed a significant amount of the $\alpha\text{-Fe}_2\text{O}_3$ volume fraction, this change signifies the change of the oxidation number from 3 to $8/3$, as the $\alpha\text{-Fe}_2\text{O}_3$ reduces to Fe_3O_4 .²⁵ The reduction of the oxidation number confirms the ability of N_2 to act as a reducing agent at high temperatures and pressures.²⁵ The reaction, which has been reported for hematite nanowires at 350°C when annealed for 1 hour, seems to be initiated at 300°C in our iron oxide nanocubes when annealed for 2 hours.²⁶ Here both inert gases did not show significant phase changes from the AP. Though significant morphological changes were absent in all the samples post-annealing, a chain formation was observed, in the annealed samples is understood to be due to the dipole-dipole interactions between the NCs with the annihilation of the surfactants.²⁷ This chain formation can be advantageous for hyperthermia treatments as it tends to increase the specific absorption rate (SAR) values with the enhancement in anisotropic interactions.^{23,24,28–30}

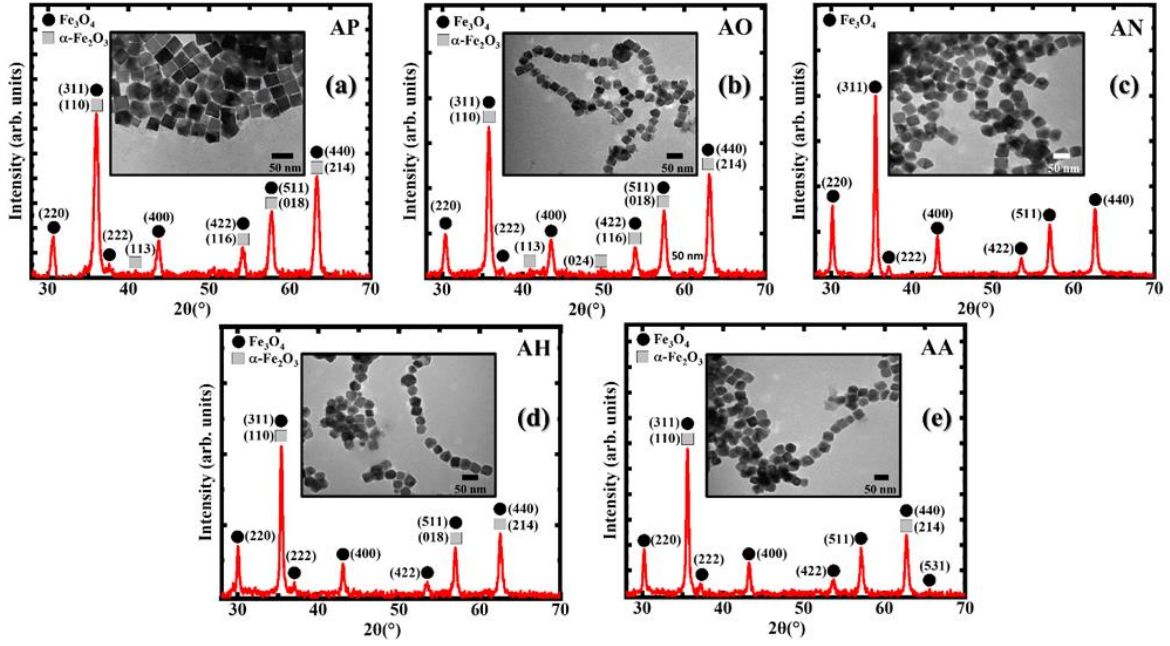


Figure 1: XRD patterns and the TEM images (inset) of (a) the as-prepared iron oxide nanocubes, (b) the iron oxide nanocubes annealed in O_2 , (c) the iron oxide nanocubes annealed in N_2 , (d) the iron oxide nanocubes annealed in He, and (e) the iron oxide nanocubes annealed in Ar.

3.2. Magnetic Properties

Temperature-dependent magnetization, $M(T)$ measurements were carried out between 10-300 K following the zero-field cooled (ZFC), field-cooled cooling (FCC), and field-cooled warming (FCW) protocols in the presence of a 0.05 T magnetic field. The Verwey transition (VT), a first-order metal-insulator transition where the crystalline phase changes from high-temperature cubic to low-temperature monoclinic indicative of the Fe_3O_4 phase, is observed in all the samples except the sample annealed in O_2 (AO) between $109\text{ K} \leq T_V \leq 121\text{ K}$.^{31–33} The sharpness of the transition which translates the crystallinity of the Fe_3O_4 phase can be observed to increase with annealing in the presence of N_2 (AN), He (AH), and Ar (AA), with the exception for the AO. The AO is understood to be oxidized in multiple stages, simultaneously with the final products of $\alpha\text{-Fe}_2O_3$, following the reaction;^{34,35}

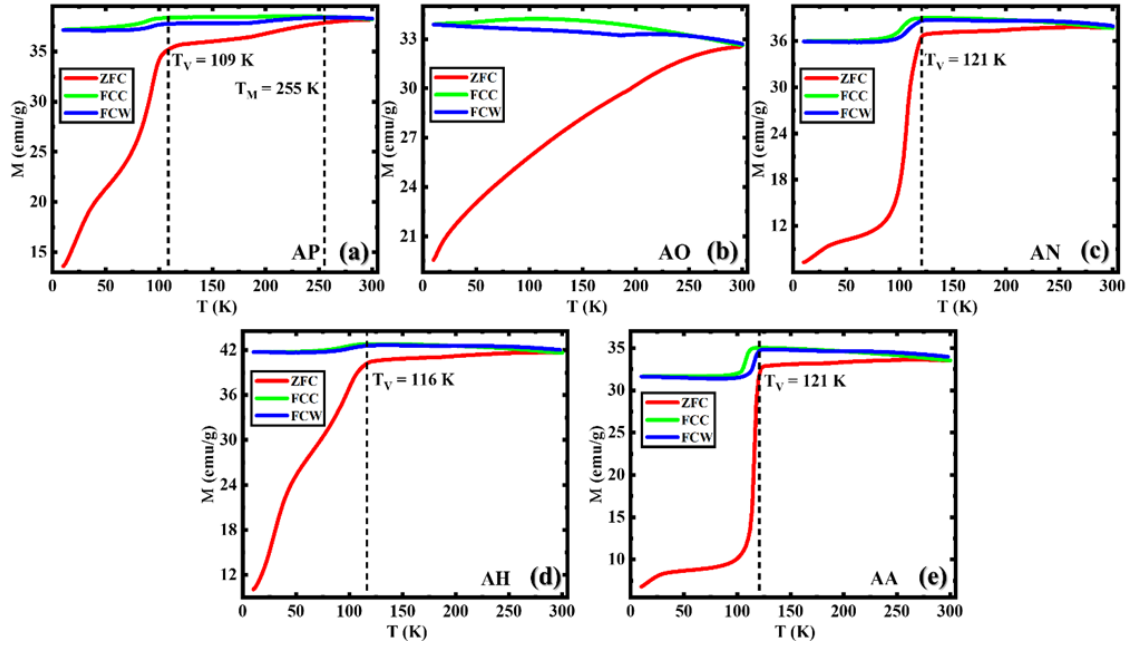


Figure 2: ZFC, FCC, and FCW $M(T)$ curves measured in an applied field of 0.05 T for (a) as-prepared, (b) annealed in O_2 , (c) annealed in N_2 , (d) annealed in He, and (e) annealed in Ar.

The inside of the structure is expected to be oxidized to $\gamma\text{-Fe}_2\text{O}_3$ -like (or $\gamma\text{-Fe}_2\text{O}_3$) phase from Fe_3O_4 which resulted in the disappearance of the VT.^{34,36-39} The absence of the VT observed in prior annealing on iron oxide nanorods by Attanayake *et al.* supports the oxidation to $\gamma\text{-Fe}_2\text{O}_3$ -like phase.^{36,40} The AN, AH, and AA which indicated the reduction in the $\alpha\text{-Fe}_2\text{O}_3$ phase indicated by the XRD data and the absence of the Morin transition (MT), are observed to show the transformation at comparative temperatures in the presence of various mixtures of gases, in our case N_2 , He, and Ar.^{41,42} Furthermore, AA indicates a slightly higher decrease in $\alpha\text{-Fe}_2\text{O}_3$ which can be observed by the absence of (018) in Fig. 1(e) and the sharpness of the VT in Fig. 2(d) compared to AH.

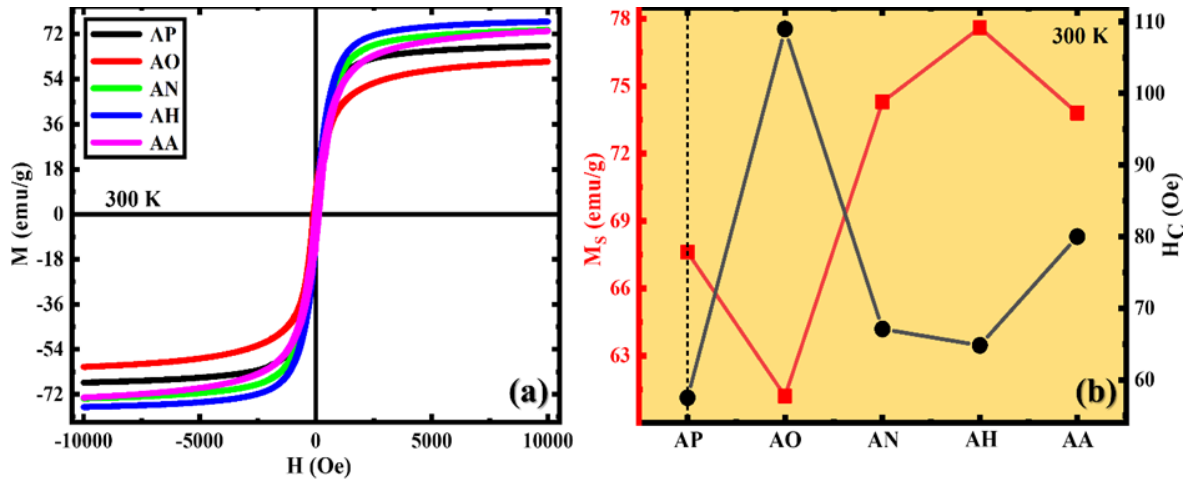


Figure 3: (a) Magnetic hysteresis loops $M(H)$ of as-prepared, annealed in O_2 , annealed in N_2 , annealed in He, and annealed in Ar, and (b) variation of magnetization at the maximum value of the applied magnetic field (M_S) and coercivity (H_C) deduced from the $M(H)$ loops.

The first-order magnetic transition, MT commonly known as the temperature-driven spin-flop transition is associated with the presence of the $\alpha\text{-Fe}_2\text{O}_3$ phase which occurs as the spin alignment changes from perpendicular to the c -axis above the T_M to parallel to the c -axis below the T_M is observable only in AP.^{43–48}

The magnetization vs. applied field $M(H)$ measurements shown in Fig. 3 were carried out at room temperature for a maximum 1 T applied field for all the samples. The magnetization at the maximum value of the applied magnetic field (M_S) decreased when moving from AP to AO but improved in all the other samples as the FiM Fe_3O_4 phase increased. Though the M_S value decreased in AO, the value did not significantly decrease as observed with sole $\alpha\text{-Fe}_2\text{O}_3$ carrying nanostructures which lie less than 10 emu/g in most cases since the sample undergoes a two-step oxidation as explained by Zheng *et al.* which leaves a significant volume fraction of the FiM Fe_3O_4 phase intact.^{34,49,50} The samples did not portray superparamagnetic features, similar to the observations made by Attanayake *et al.* but displayed an inversely proportional relationship between M_S and coercivity (H_C), which can be related to the Stoner-Wohlfarth

theory, $H_K = \frac{2K_{Ani}}{\mu_0 M_S}$; which shows that the magnetocrystalline anisotropy of a single domain particle is expected to show an inversely proportional relationship between M_S and H_K , thus the H_C change shown in Fig. 3b.^{19,51,52} The general increment H_C in all the annealed samples may be due to the magnetic hardening of the nanostructures with annealing, this is as the magnetic phases, especially the FM/FiM phases become more stable with annealing making them more resistant to demagnetization, and additionally defect formation with annealing can lead to magnetic pinning as it is a well-known defect engineering mechanism.^{53,54} A H_C of above 100 Oe was only registered in AO, understandably due to the combination of the effects; magnetic hardening, defect formation, and increased magnetic anisotropy.^{7,54,55} Tunability of the AP in terms of M_S , and H_C with varying gas types opens up the possibility for the nanostructures to be explored for the effectiveness of magnetic hyperthermia measurements with enhanced H_C and M_S separately, further tuned in accordance to varying applications such as magnetic particle imaging, magnetic tracers, etc..⁵³

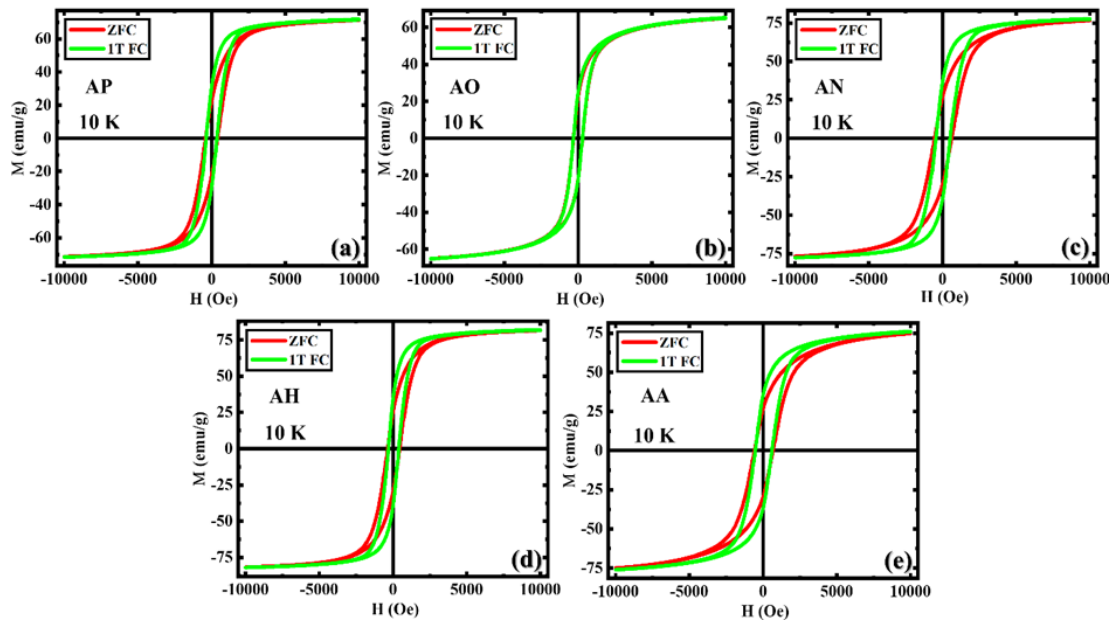


Figure 4: Magnetic Hysteresis loops $M(H)$ recorded in ZFC and FC protocols in an applied field of 1 T for (a) as-prepared, (b) annealed in O_2 , (c) annealed in N_2 , (d) annealed in He, and (e) annealed in Ar.

Low-temperature $M(H)$ measurements at 10 K showed a higher M_s compared to the 300 K typical for nanostructures as the superficial spins tend to get better aligned with the applied magnetic field at lower temperatures as the thermal energy is lower, observed in smaller nanostructures with a high surface-to-volume ratio, which follows the Kneller's law which predicts an inversely proportional relationship between H_C and T .^{56,57} The ZFC and FC protocols applied on the nanostructures did not yield an exchange bias effect at the FiM Fe_3O_4 and AFM $\alpha-Fe_2O_3$ interfaces, understood to be due to the negligible interfacial interactions due to frozen spins.^{19,37} The pinning effect is observed in all the samples and is the smallest in the AO, which may be due to the formation of a $\gamma-Fe_2O_3$ -like phase similar to the observations made with iron oxide nanorods annealed with oxygen.³⁷

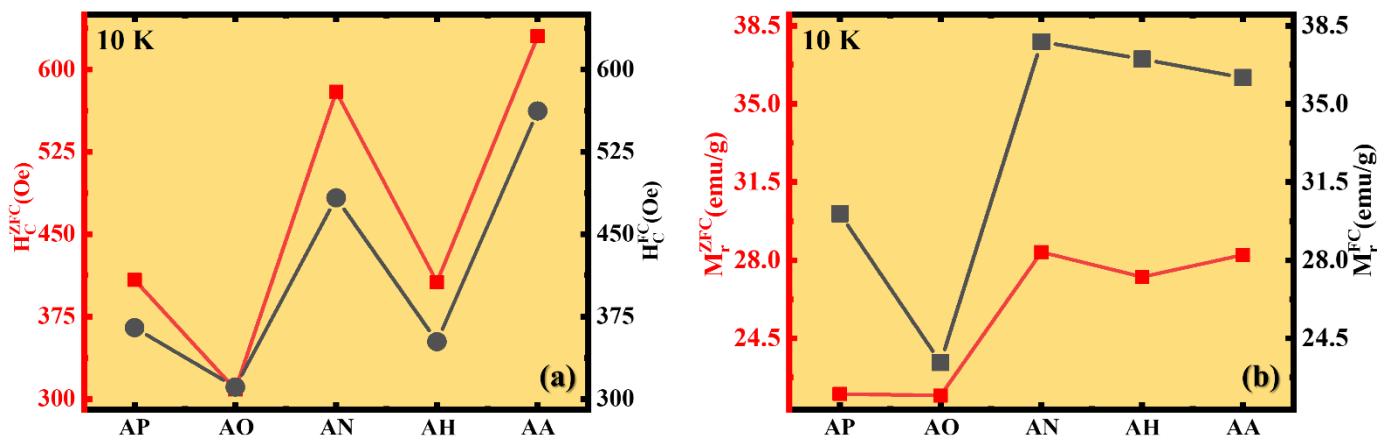


Figure 5: (a) H_C values obtained at 10 K for ZFC and FC configurations, and (b) M_r at 10 K for ZFC and FC configurations.

The H_C with and without the application of the 2T field shows the separation with the observed biphases. The ZFC protocol which lets the spins be randomly oriented while being cooled down to the low temperature will possess a higher H_C as the antiferromagnetic exchange coupling will pin the ferrimagnetic moments at the interface, but with the application of the FC protocol, the ferrimagnetic phase will align minimizing the interfacial pinning with the assistance of the cubic structure. The AO is the only sample that does not show a significant difference between the said two protocols with its dominant $\gamma-Fe_2O_3$ -like phase, which does

not possess the regular biphasic behavior in magnetic measurements. A similar observation is observed in the magnetization curves in Fig. 5(b) with AO.

3.1. Magnetic Hyperthermia

Figure 6(a-c) depicts the usage of samples in hyperthermia measurements, namely, the heating $T(t)$ curves, at varying fields for a 300-second window, a relatively short period, which has been understood to be comparatively more effective in conjunction with radiation therapy at moderately lethal temperatures which are higher than the general hyperthermia window of 40-44 °C.⁵⁸⁻⁶¹ Additionally, longer treatment periods are also associated with patient fatigue, adjacent healthy tissue destruction, and changes in the body conditions which can lead to complex reactions, adversely affecting the health and well-being of a patient.⁶² Nanoparticle introduction was kept at 1 mg/mL, due to the tendency of instinctive reactions leading to adverse conditions, irrespective of the compatibility.^{63,64} In the in-vitro study to ensure the performance of the nanoparticles in par or closer to the environment inside the body, a 2% by weight agar, a medium denser than water was used.^{9,65} The SAR value of the heating curves was calculated using the initial slope method of the heating curve with the following equation;

$$SAR = \frac{\Delta T}{\Delta t} \frac{C_p}{\phi}$$

The method devised, assumes a homogenous sample temperature and negligible heat loss at certain time intervals at the start of the alternating magnetic field.^{66,67} Here the $\Delta T/\Delta t$ gives the rate of change of temperature, and C_p indicates the specific heat capacity of the liquid medium. Here, the agar at 2% by weight is assumed not to have significantly changed its specific heat capacity and thus 4.186 J/(g °C), the heat capacity of water is used. The symbol ϕ indicates the mass of magnetic material per unit mass of liquid, which essentially gives the concentration used in the measurements.

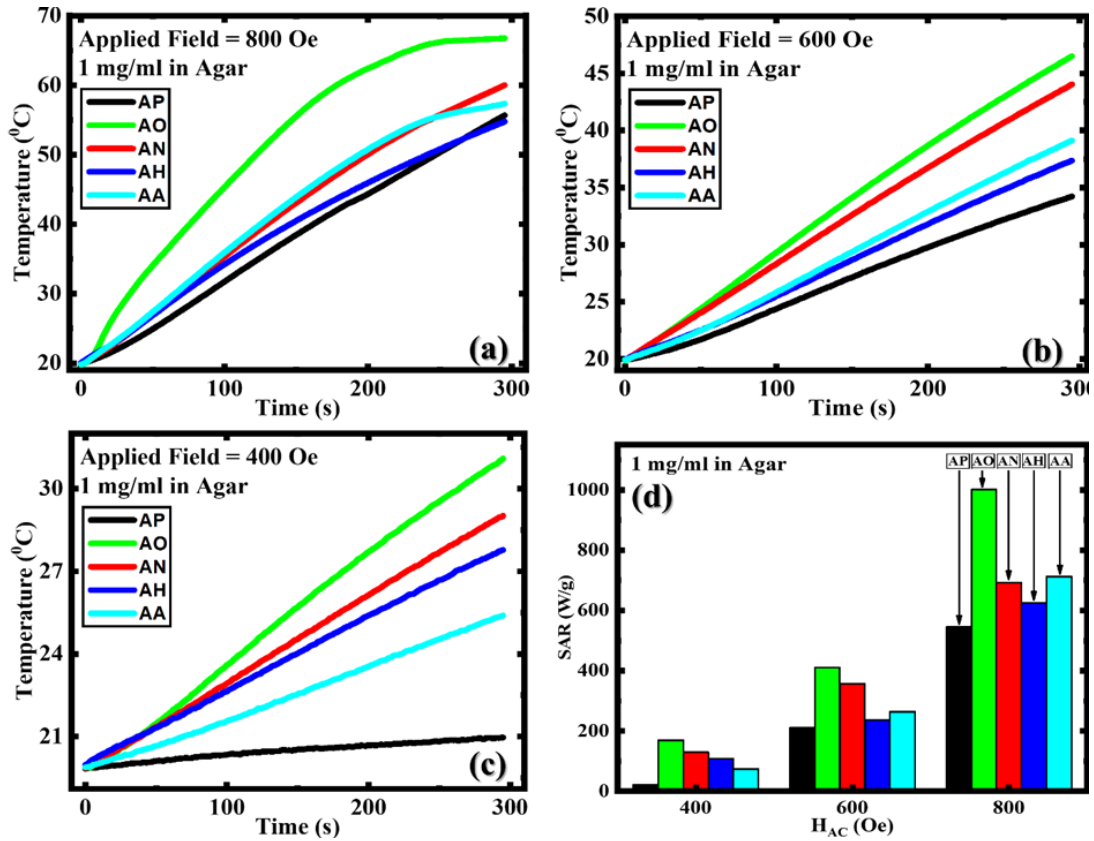


Figure 6: Heating curves of samples with concentration 1 mg/mL in agar, measured at 310 kHz frequency at (a) 800 Oe, (b) 600 Oe, (c) 400 Oe, and (d) SAR of all the samples measured at 400, 600, and 800 Oe.

It can be seen in Fig. 6d that all the samples in general showed significant improvement in heating potential and SAR values compared to the AP, while the AO showed an exceptional enhancement. The general enhancement of heating capabilities can be due to defect enhancement and increased grain size which in turn led to increased anisotropy.^{53,68} The AO showed the highest SAR value in all the applied magnetic fields with the highest of 1001 W/g at 800 Oe (Fig. 6d, & **Table 1**), which is almost four times higher than that reported in FeO/Fe₃O₄ nanocubes synthesized by Khurshid *et al.*²¹ Further when compared with the FiM iron oxide nanocubes of a similar size synthesized by Nemati *et al.* which showed almost the same magnetic properties compared to the AP sample (refer **Table 1**), the annealing was observed to have significantly increased the SAR in all the samples.⁸ This suggests and re-

affirms the already understood phenomena of SAR enhancement with the increment of M_S and H_C .^{69–71} In our study, the 34 nm nanocubes were used eliminating the variability of size and shape parameters. The adjusted annealing environments between the AO and AN samples clearly show that the M_S and H_C play a pivotal role in altering the SAR, but the enhanced H_C in AO is observed to lead to a higher SAR value compared to the M_S improved in the AN. Table 1 summarizes the change in H_C , M_S , and SAR in all the samples and highlights the exceptional SAR value observed in AO which possesses the highest H_C underscoring the general relation between H_C and SAR which supersedes the effect of M_S .

Table 1: Magnetic and Hyperthermia properties of the sample set at 300 K.

Sample	H_C (Oe)	M_S (emu/g)	SAR in Agar @ 800 Oe (W/g)
<i>30 nm Nanocubes</i> ⁸	33.7	67.5	~540
AP	57.5	67.6	544
AO	109	61.2	1001
AN	67.1	74.3	692.8
AH	64.8	77.6	624.4
AA	80	73.8	712.3

4. Conclusion

The phase tunability of 34 nm iron oxide nanocubes with different types of gases enabled the enhancement of different fundamental magnetic properties, such as coercivity, saturation magnetization, and crystallinity. The enhancement of the specific absorption rate in all the samples with annealing, along with the general increment of coercivity reflected how magnetic anisotropy can affect magnetic hyperthermia efficiency. Comparing the annealing-induced changes in the coercivity and saturation magnetization, which are well-known parameters in tuning the specific absorption rate, it is observed that the former plays a larger

role as the value in all the three tested applied magnetic fields were significantly higher in the AO, with enhanced H_C .

Acknowledgments

The research was supported by the US Department of Energy, Office of Basic Energy Sciences, Division of Material Science and Engineering under Award No. DE-FG02-07ER46438.

References

- ¹ E.M. Materón, C.M. Miyazaki, O. Carr, N. Joshi, P.H.S. Picciani, C.J. Dalmaschio, F. Davis, and F.M. Shimizu, “Magnetic nanoparticles in biomedical applications: A review,” *Applied Surface Science Advances* **6**, 100163 (2021).
- ² P.M. Martins, A.C. Lima, S. Ribeiro, S. Lanceros-Mendez, and P. Martins, “Magnetic Nanoparticles for Biomedical Applications: From the Soul of the Earth to the Deep History of Ourselves,” *ACS Appl Bio Mater* **4**(8), 5839–5870 (2021).
- ³ G.C. Lavorato, R. Das, J. Alonso Masa, M.H. Phan, and H. Srikanth, “Hybrid magnetic nanoparticles as efficient nanoheaters in biomedical applications,” *Nanoscale Adv* **3**(4), 867–888 (2021).
- ⁴ C. Kons, K.L. Krycka, J. Robles, N. Ntallis, M. Pereiro, M.H. Phan, H. Srikanth, J.A. Borchers, and D.A. Arena, “Influence of Hard/Soft Layer Ordering on Magnetization Reversal of Bimagnetic Nanoparticles: Implications for Biomedical/Theranostic Applications,” *ACS Appl Nano Mater* **6**(13), 10986–11000 (2023).
- ⁵ P.M. Martins, A.C. Lima, S. Ribeiro, S. Lanceros-Mendez, and P. Martins, “Magnetic Nanoparticles for Biomedical Applications: From the Soul of the Earth to the Deep History of Ourselves,” *ACS Appl Bio Mater* **4**(8), 5839–5870 (2021).
- ⁶ G.C. Lavorato, R. Das, J. Alonso Masa, M.H. Phan, and H. Srikanth, “Hybrid magnetic nanoparticles as efficient nanoheaters in biomedical applications,” *Nanoscale Adv* **3**(4), 867–888 (2021).
- ⁷ Z. Nemati, J. Alonso, L.M. Martinez, H. Khurshid, E. Garaio, J.A. Garcia, M.H. Phan, and H. Srikanth, “Enhanced Magnetic Hyperthermia in Iron Oxide Nano-Octopods: Size and Anisotropy Effects,” *Journal of Physical Chemistry C* **120**(15), 8370–8379 (2016).

- ⁸ Z. Nemati, J. Alonso, I. Rodrigo, R. Das, E. Garaio, J.Á. García, I. Orue, M.H. Phan, and H. Srikanth, “Improving the Heating Efficiency of Iron Oxide Nanoparticles by Tuning Their Shape and Size,” *Journal of Physical Chemistry C* **122**(4), 2367–2381 (2018).
- ⁹ R. Das, J. Alonso, Z. Nemati Porshokouh, V. Kalappattil, D. Torres, M.H. Phan, E. Garaio, J.Á. García, J.L. Sanchez Llamazares, and H. Srikanth, “Tunable High Aspect Ratio Iron Oxide Nanorods for Enhanced Hyperthermia,” *Journal of Physical Chemistry C* **120**(18), 10086–10093 (2016).
- ¹⁰ G.C. Lavorato, R. Das, Y. Xing, J. Robles, F.J. Litterst, E. Baggio-Saitovitch, M.H. Phan, and H. Srikanth, “Origin and Shell-Driven Optimization of the Heating Power in Core/Shell Bimagnetic Nanoparticles,” *ACS Appl Nano Mater* **3**(2), 1755–1765 (2020).
- ¹¹ S. Chandra, R. Das, V. Kalappattil, T. Eggers, C. Harnagea, R. Nechache, M.H. Phan, F. Rosei, and H. Srikanth, “Epitaxial magnetite nanorods with enhanced room temperature magnetic anisotropy,” *Nanoscale* **9**(23), 7858–7867 (2017).
- ¹² D.J. Denmark, R.H. Hyde, C. Gladney, M.H. Phan, K.S. Bisht, H. Srikanth, P. Mukherjee, and S. Witanachchi, “Photopolymerization-based synthesis of iron oxide nanoparticle embedded PNIPAM nanogels for biomedical applications,” *Drug Deliv* **24**(1), 1317–1324 (2017).
- ¹³ D.J. Denmark, R.H. Hyde, C. Gladney, M.H. Phan, K.S. Bisht, H. Srikanth, P. Mukherjee, and S. Witanachchi, “Photopolymerization-based synthesis of iron oxide nanoparticle embedded PNIPAM nanogels for biomedical applications,” *Drug Deliv* **24**(1), 1317–1324 (2017).
- ¹⁴ D. Gandia, L. Gandarias, I. Rodrigo, J. Robles-García, R. Das, E. Garaio, J.Á. García, M.H. Phan, H. Srikanth, I. Orue, J. Alonso, A. Muela, and M.L. Fdez-Gubieda, “Unlocking

the Potential of Magnetotactic Bacteria as Magnetic Hyperthermia Agents,” *Small* **15**(41), 1902626 (2019).

¹⁵ P.Q. Thong, L.T.T. Huong, N.D. Tu, H.T.M. Nhung, L. Khanh, D.H. Manh, P.H. Nam, N.X. Phuc, J. Alonso, J. Qiao, S. Sridhar, H.P. Thu, M.H. Phan, and N.T.K. Thanh, “Multifunctional nanocarriers of Fe₃O₄@PLA-PEG/curcumin for MRI, magnetic hyperthermia and drug delivery,” *Nanomedicine* **17**(22), 1677–1693 (2022).

¹⁶ X. Ge, J. Mohapatra, E. Silva, G. He, L. Gong, T. Lyu, R.P. Madhogaria, X. Zhao, Y. Cheng, A.M. Al-Enizi, A. Nafady, J. Tian, J.P. Liu, M.H. Phan, F. Taraballi, R.I. Pettigrew, and S. Ma, “Metal–Organic Framework as a New Type of Magnetothermally-Triggered On-Demand Release Carrier,” *Small*, 2306940 (2023).

¹⁷ A.S. Thakor, J. V. Jokerst, P. Ghanouni, J.L. Campbell, E. Mittra, and S.S. Gambhir, “Clinically Approved Nanoparticle Imaging Agents,” *Journal of Nuclear Medicine* **57**(12), 1833–1837 (2016).

¹⁸ F. Soetaert, P. Korangath, D. Serantes, S. Fiering, and R. Ivkov, “Cancer therapy with iron oxide nanoparticles: Agents of thermal and immune therapies,” *Adv Drug Deliv Rev* **163–164**, 65–83 (2020).

¹⁹ S.B. Attanayake, A. Chanda, R. Das, N. Kapuruge, H.R. Gutierrez, M.H. Phan, and H. Srikanth, “Emergent magnetism and exchange bias effect in iron oxide nanocubes with tunable phase and size,” *Journal of Physics: Condensed Matter* **34**(49), 495301 (2022).

²⁰ C. Martinez-Boubeta, K. Simeonidis, A. Makridis, M. Angelakeris, O. Iglesias, P. Guardia, A. Cabot, L. Yedra, S. Estradé, F. Peiró, Z. Saghi, P.A. Midgley, I. Conde-Leborán, D. Serantes, and D. Baldomir, “Learning from Nature to Improve the Heat Generation of Iron-Oxide Nanoparticles for Magnetic Hyperthermia Applications,” *Scientific Reports* **2013** 3:1 **3**(1), 1–8 (2013).

- ²¹ H. Khurshid, J. Alonso, Z. Nematy, M.H. Phan, P. Mukherjee, M.L. Fdez-Gubieda, J.M. Barandiarán, and H. Srikanth, “Anisotropy effects in magnetic hyperthermia: A comparison between spherical and cubic exchange-coupled FeO/Fe₃O₄ nanoparticles,” *J Appl Phys* **117**(17), 17A337 (2015).
- ²² D. Kim, N. Lee, M. Park, B.H. Kim, K. An, and T. Hyeon, “Synthesis of uniform ferrimagnetic magnetite nanocubes,” *J Am Chem Soc* **131**(2), 454–455 (2009).
- ²³ S. Barber-Zucker, N. Keren-Khadmy, and R. Zarivach, “From invagination to navigation: The story of magnetosome-associated proteins in magnetotactic bacteria,” *Protein Science* **25**(2), 338–351 (2016).
- ²⁴ S. Kralj, and S. Marchesan, “Bioinspired Magnetic Nanochains for Medicine,” *Pharmaceutics* 2021, Vol. 13, Page 1262 **13**(8), 1262 (2021).
- ²⁵ H. Tokoro, S. Fujii, and T. Oku, “Iron Nanoparticles Coated with Boron Nitride Nanolayers Synthesized by a Solid Phase Reaction,” *IEEE Trans Magn* **39**(5 II), 2761–2763 (2003).
- ²⁶ Y. Ling, G. Wang, H. Wang, Y. Yang, and Y. Li, “Low-Temperature Activation of Hematite Nanowires for Photoelectrochemical Water Oxidation,” *ChemSusChem* **7**(3), 848–853 (2014).
- ²⁷ K. Rout, M. Mohapatra, S. Layek, A. Dash, H.C. Verma, and S. Anand, “The influence of precursors on phase evolution of nano iron oxides/oxyhydroxides: optical and magnetic properties,” *New Journal of Chemistry* **38**(8), 3492–3506 (2014).
- ²⁸ D. Niculaes, A. Lak, G.C. Anyfantis, S. Marras, O. Laslett, S.K. Avugadda, M. Cassani, D. Serantes, O. Hovorka, R. Chantrell, and T. Pellegrino, “Asymmetric Assembling of Iron Oxide Nanocubes for Improving Magnetic Hyperthermia Performance,” *ACS Nano* **11**, 2023 (2017).

- ²⁹ R. Le Fèvre, M. Durand-Dubief, I. Chebbi, C. Mandawala, F. Lagroix, J.P. Valet, A. Idbah, C. Adam, J.Y. Delattre, C. Schmitt, C. Maake, F. Guyot, and E. Alphanbéry, “Enhanced antitumor efficacy of biocompatible magnetosomes for the magnetic hyperthermia treatment of glioblastoma,” *Theranostics* **7**(18), 4618 (2017).
- ³⁰ E. Alphanbéry, I. Chebbi, F. Guyot, and M. Durand-Dubief, “Use of bacterial magnetosomes in the magnetic hyperthermia treatment of tumours: A review,” *International Journal of Hyperthermia* **29**(8), 801–809 (2013).
- ³¹ E.J.W. Verwey, “Electronic conduction of magnetite (Fe₃O₄) and its transition point at low temperatures [5],” *Nature* **144**(3642), 327–328 (1939).
- ³² F. Walz, “The Verwey transition - A topical review,” *Journal of Physics Condensed Matter* **14**(12), (2002).
- ³³ Ö. Özdemir, D.J. Dunlop, and B.M. Moskowitz, “Changes in remanence, coercivity and domain state at low temperature in magnetite,” *Earth Planet Sci Lett* **194**(3–4), 343–358 (2002).
- ³⁴ H. Zheng, J. Schenk, D. Spreitzer, T. Wolfinger, and O. Daghighaleh, “Review on the Oxidation Behaviors and Kinetics of Magnetite in Particle Scale,” *Steel Res Int* **92**(8), 2000687 (2021).
- ³⁵ A. V. Anupama, W. Keune, and B. Sahoo, “Thermally induced phase transformation in multi-phase iron oxide nanoparticles on vacuum annealing,” *J Magn Magn Mater* **439**, 156–166 (2017).
- ³⁶ S.B. Attanayake, A. Chanda, R. Das, M.H. Phan, and H. Srikanth, “Effects of annealing temperature on the magnetic properties of highly crystalline biphasic iron oxide nanorods,” *AIP Adv* **13**(2), 025333 (2023).

- ³⁷ S.B. Attanayake, A. Chanda, T. Hulse, R. Das, M.-H. Phan, and H. Srikanth, “Competing Magnetic Interactions and Field-Induced Metamagnetic Transition in Highly Crystalline Phase-Tunable Iron Oxide Nanorods,” *Nanomaterials* 2023, Vol. 13, Page 1340 **13**(8), 1340 (2023).
- ³⁸ J.B. Yang, X.D. Zhou, W.B. Yelon, W.J. James, Q. Cai, K. V. Gopalakrishnan, S.K. Malik, X.C. Sun, and D.E. Nikles, “Magnetic and structural studies of the Verwey transition in Fe₃- δ O₄ nanoparticles,” *J Appl Phys* **95**(11), 7540 (2004).
- ³⁹ C. Schmitz-Antoniak, D. Schmitz, A. Warland, M. Darbandi, S. Haldar, S. Bhandary, B. Sanyal, O. Eriksson, and H. Wende, “Suppression of the Verwey Transition by Charge Trapping,” *Ann Phys* **530**(3), 1700363 (2018).
- ⁴⁰ S.B. Attanayake, A. Chanda, R. Das, M.H. Phan, and H. Srikanth, “Emergent magnetic properties of biphasic iron oxide nanorods,” *AIP Adv* **12**(3), 035136 (2022).
- ⁴¹ J.P. Gaviría, A. Bohé, A. Pasquevich, and D.M. Pasquevich, “Hematite to magnetite reduction monitored by Mössbauer spectroscopy and X-ray diffraction,” *Physica B Condens Matter* **389**(1), 198–201 (2007).
- ⁴² W.W. Wang, Y.J. Zhu, and M.L. Ruan, “Microwave-assisted synthesis and magnetic property of magnetite and hematite nanoparticles,” *Journal of Nanoparticle Research* **9**(3), 419–426 (2007).
- ⁴³ J.O. Artman, J.C. Murphy, and S. Foner, “Magnetic Anisotropy in Antiferromagnetic Corundum-Type Sesquioxides,” *Physical Review* **138**(3A), A912 (1965).
- ⁴⁴ S. Mitra, S. Das, S. Basu, P. Sahu, and K. Mandal, “Shape- and field-dependent Morin transitions in structured α -Fe₂O₃,” *J Magn Magn Mater* **321**(18), 2925–2931 (2009).

- ⁴⁵ S. Mørup, D.E. Madsen, C. Frandsen, C.R.H. Bahl, and M.F. Hansen, “Experimental and theoretical studies of nanoparticles of antiferromagnetic materials,” *Journal of Physics: Condensed Matter* **19**(21), 213202 (2007).
- ⁴⁶ Ö. Özdemir, D.J. Dunlop, and T.S. Berquó, “Morin transition in hematite: Size dependence and thermal hysteresis,” *Geochemistry, Geophysics, Geosystems* **9**(10), 10–11 (2008).
- ⁴⁷ N. Shimomura, S.P. Pati, Y. Sato, T. Nozaki, T. Shibata, K. Mibu, and M. Sahashi, “Morin transition temperature in (0001)-oriented α -Fe₂O₃ thin film and effect of Ir doping,” *J Appl Phys* **117**(17), 17C736 (2015).
- ⁴⁸ J. Wang, V. Aguilar, L. Li, F. gen Li, W. zhong Wang, and G. meng Zhao, “Strong shape-dependence of Morin transition in α -Fe₂O₃ single-crystalline nanostructures,” *Nano Res* **8**(6), 1906–1916 (2015).
- ⁴⁹ Q.J. Sun, X.G. Lu, and G.Y. Liang, “Controlled template-free hydrothermal synthesis of hematite nanoplatelets,” *Mater Lett* **64**(18), 2006–2008 (2010).
- ⁵⁰ J. Jacob, and M. Abdul Khadar, “VSM and Mössbauer study of nanostructured hematite,” *J Magn Magn Mater* **322**(6), 614–621 (2010).
- ⁵¹ Q. Chen, and Z.J. Zhang, “Size-dependent superparamagnetic properties of MgFe₂O₄ spinel ferrite nanocrystallites,” *Appl Phys Lett* **73**(21), 3156–3158 (1998).
- ⁵² R.R. Coore, S. Love, C.R. Helps, and M.H. Anil, “Frequency of brain tissue embolism associated with captive bolt gun stunning of sheep.,” *Foodborne Pathog Dis* **1**(4), 291–294 (2004).
- ⁵³ A. Lak, S. Disch, and P. Bender, “Embracing Defects and Disorder in Magnetic Nanoparticles,” *Advanced Science* **8**(7), 2002682 (2021).

- ⁵⁴ B. Muzzi, E. Lottini, N. Yaacoub, D. Peddis, G. Bertoni, C. De Julián Fernández, C. Sangregorio, and A. López-Ortega, “Hardening of Cobalt Ferrite Nanoparticles by Local Crystal Strain Release: Implications for Rare Earth Free Magnets,” *ACS Appl Nano Mater* **5**(10), 14871–14881 (2022).
- ⁵⁵ S. Singh, S. Munjal, and N. Khare, “Strain/defect induced enhanced coercivity in single domain CoFe₂O₄ nanoparticles,” *J Magn Magn Mater* **386**, 69–73 (2015).
- ⁵⁶ E.F. Kneller, and F.E. Luborsky, “Particle Size Dependence of Coercivity and Remanence of Single-Domain Particles,” *J Appl Phys* **34**(3), 656 (2004).
- ⁵⁷ I. Nkurikiyimfura, Y. Wang, B. Safari, and E. Nshingabigwi, “Temperature-dependent magnetic properties of magnetite nanoparticles synthesized via coprecipitation method,” *J Alloys Compd* **846**, 156344 (2020).
- ⁵⁸ S.M. Waldow, and T.J. Dougherty, “Interaction of Hyperthermia and Photoradiation Therapy,” *Radiat Res* **97**(2), 380–385 (1984).
- ⁵⁹ J. Crezee, N.A.P. Franken, and A.L. Oei, “Hyperthermia-Based Anti-Cancer Treatments,” *Cancers* 2021, Vol. 13, Page 1240 **13**(6), 1240 (2021).
- ⁶⁰ H.P. Kok, P. Wust, P.R. Stauffer, F. Bardati, G.C. van Rhoon, and J. Crezee, “Current state of the art of regional hyperthermia treatment planning: a review,” *Radiation Oncology* 2015 **10**:1 **10**(1), 1–14 (2015).
- ⁶¹ D. Ortega, and Q.A. Pankhurst, “Magnetic hyperthermia,” 60–88 (2012).
- ⁶² D. Arora, M. Skliar, and R.B. Roemer, “Model-predictive control of hyperthermia treatments,” *IEEE Trans Biomed Eng* **49**(7), 629–639 (2002).

- ⁶³ P. Moroz, S.K. Jones, B.N. Gray, P. Morozy, S.K. Jonesz, and B.N. Grayz, “Magnetically mediated hyperthermia: current status and future directions,” *International Journal of Hyperthermia* **18**(4), 267–284 (2002).
- ⁶⁴ G. Bellizzi, O.M. Bucci, and G. Chirico, “Numerical assessment of a criterion for the optimal choice of the operative conditions in magnetic nanoparticle hyperthermia on a realistic model of the human head,” *International Journal of Hyperthermia* **32**(6), 688–703 (2016).
- ⁶⁵ B.B. Lahiri, S. Ranoo, and J. Philip, “Effect of orientational ordering of magnetic nanoemulsions immobilized in agar gel on magnetic hyperthermia,” *J Magn Magn Mater* **451**, 254–268 (2018).
- ⁶⁶ I. Andreu, and E. Natividad, “Accuracy of available methods for quantifying the heat power generation of nanoparticles for magnetic hyperthermia,” *Int J Hyperthermia* **29**(8), 739–751 (2013).
- ⁶⁷ I. Hilger, K. Frühauf, W. Andrä, R. Hiergeist, R. Hergt, and W.A. Kaiser, “Heating potential of iron oxides for therapeutic purposes in interventional radiology,” *Acad Radiol* **9**(2), 198–202 (2002).
- ⁶⁸ Z.N. Kayani, S. Arshad, S. Riaz, and S. Naseem, “Synthesis of Iron Oxide Nanoparticles by Sol-Gel Technique and Their Characterization,” *IEEE Trans Magn* **50**(8), (2014).
- ⁶⁹ M. Ma, Y. Wu, J. Zhou, Y. Sun, Y. Zhang, and N. Gu, “Size dependence of specific power absorption of Fe₃O₄ particles in AC magnetic field,” *J Magn Magn Mater* **268**(1–2), 33–39 (2004).
- ⁷⁰ J. Mohapatra, F. Zeng, K. Elkins, M. Xing, M. Ghimire, S. Yoon, S.R. Mishra, and J.P. Liu, “Size-dependent magnetic and inductive heating properties of Fe₃O₄ nanoparticles: scaling

laws across the superparamagnetic size,” *Physical Chemistry Chemical Physics* **20**(18), 12879–12887 (2018).

⁷¹ X.L. Liu, H.M. Fan, J.B. Yi, Y. Yang, E.S.G. Choo, J.M. Xue, D. Di Fan, and J. Ding, “Optimization of surface coating on Fe₃O₄ nanoparticles for high performance magnetic hyperthermia agents,” *J Mater Chem* **22**(17), 8235–8244 (2012).